Coverage of coherent output states in parallel-coupled dual-racetrack microresonators

Wei Jiang (江 伟)[1,2,3] and Yating Zhou (周亚亭)[2,3,4,*]

[1]*College of Engineering and Applied Sciences & National Laboratory of Solid State Microstructures, Nanjing University, Nanjing 210093, China*

[2]*Department of Electrical and Computer Engineering, Rutgers University, Piscataway, New Jersey 08854, USA*

[3]*Institute for Advanced Materials, Devices, and Nanotechnology, Rutgers University, Piscataway, New Jersey 08854, USA*

[4]*School of Mathematics and Physics & Chemical Engineering, Changzhou Institute of Technology, Changzhou 213002, China*

**Corresponding author: zhouyt@czu.cn*

Received June 28, 2016; accepted August 26, 2016; posted online September 30, 2016

Parallel-coupled dual-racetrack silicon microresonators can potentially be used for quadrature amplitude modulation. We analyze the evolution of the coverage of coherent output states of devices with varying device parameters. As the coupling constant increases, the coverage of coherent states initially improves then degrades, which is unexpected based on a prior preference for overcoupling. Increasing the quality factor generally improves the coverage. The influence of the refractive index modulation is found to saturate after reaching a certain level. Analytic formulas are developed to provide insight into the coverage evolution. These results are fairly robust against a small asymmetry of device parameters.

OCIS codes: 230.5750, 250.7360, 250.4745.
doi: 10.3788/COL201614.102304.

Advanced optical modulation formats such as quadrature phase-shift keying and quadrature amplitude modulation could offer significant advantages for optical communications[1]. Recently, microresonator-based silicon modulators[2–6] have emerged as an ideal candidate for optical modulation devices due to their compact size, low power consumption, and ease of integration with on-chip driving circuitries. Microring resonator-based modulators have been studied for advanced modulation formats[7,8]. We have proposed a novel parallel-coupled dual-racetrack (PCDR) microresonator structure[9], illustrated in Fig. 1, for phase-shift keying and M-ary quadrature amplitude modulation (QAM). Two identical silicon racetrack resonators are symmetrically parallel coupled to a middle waveguide. The modulator can be fabricated on a silicon-on-insulator (SOI) wafer. The carriers can be injected or depleted from the resonators using a PIN diode or a metal-oxide-semiconductor capacitor embedded in a silicon waveguide. The plasma dispersion effect of the injected carriers modifies the refractive index Δn_1, Δn_3 in each racetrack resonator, which affects the cross-coupled resonances of the two racetrack resonators. A salient feature of this structure is that the coherent cross coupling between the two racetrack resonators mediated by the middle waveguide drastically modifies the amplitude/phase characteristics of resonance. This enables arbitrary M-ary quadrature signal generations such as quadrature phase-shift keying (QPSK) and 16-QAM. The entire structure can be extremely compact ($\sim$14 μm × 10 μm), which is a significant advantage compared to conventional QPSK modulators.

A key performance feature of this structure is that it can achieve very large coverage of all the possible states for the coherent output field. It has been found qualitatively that overcoupling tends to be beneficial to a large coverage of all possible states[9]. Other than this, very little is known about how to optimize various parameters to achieve a large coverage of all possible coherent output states. In this work, we show that within the overcoupling regime the coverage of output states depends on the coupling constant in a complex manner, and excessively strong coupling is not conducive to achieving a large coverage. The quantitative result is unexpected and it reveals that refined design and analysis is necessary to choose a proper coupling constant rather than simply going for very strong coupling. On the other hand, an increasing quality factor tends to always be beneficial to a large coverage. We develop an analytic theory that explains these dependencies accurately and provide insight into the device performance. Furthermore, the influence of the level of the refractive index modulation is found to saturate after

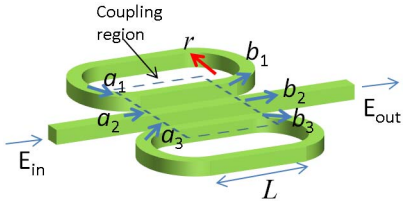

Fig. 1. Schematic drawing of PCDR resonators.

reaching a certain level, which offers useful information for efficient operation of the device.

We start with a recapitulation of the key points of the PCDR resonators[9]. The coupling between the two racetrack resonators and the middle waveguide in Fig. 1 can be described by multiwaveguide coupling theory. The solution of the coupled mode equations yields a set of linear relations between a_n and b_n, which are the normalized input and output amplitudes labeled in Fig. 1. The linear relations depend on the parameters $c_1 = \frac{1}{2}\cos(\sqrt{2}\kappa L)$, $c_2 = \frac{1}{\sqrt{2}} i \sin(\sqrt{2}\kappa L)$, where κ is the coupling constant. The strength of the cross coupling between the two racetrack resonators mediated by the through waveguide is given by $|c_1 - 1/2|$. In addition, light propagation along a racetrack gives rise to another set of relations between a_n and b_n. Assuming a unity input amplitude $a_2 = 1$, the output amplitude b_2 can be solved as

$$b_2 = e^{i\phi}\left[-1 + \frac{2(c_1 + 1/2)}{(1/2 - c_1)(1/\Delta u_1 + 1/\Delta u_3) + 1}\right], \quad (1)$$

where $\phi = \beta L$, β is the propagation constant, and

$$\Delta u_n \equiv \frac{1}{e^{i\phi + i\theta_n}\eta_n} - 1, \qquad n = 1, 3, \quad (2)$$

where $\eta_n < 1$ is the amplitude attenuation along a racetrack and θ_n is a phase shift. The critical coupling condition can be obtained by setting $b_2 = 0$ in Eq. (1). Without modulation ($\Delta u_1 = \Delta u_3$), this condition is given by

$$\eta_1 = 2c_1 = \cos\sqrt{2}\kappa L. \quad (3)$$

Under modulation, the phase shift θ_n in each racetrack will be a linear function of the refractive index changes Δn_n due to carrier injection or extraction in the respective racetrack resonator. Therefore, the output amplitude b_2 depends on Δn_n through the phase-shift terms. Detailed calculations show that the modulated phase and amplitude vanishes under the conditions

$$\phi + \theta_1 = 2m_1\pi - \Delta\theta, \qquad \phi + \theta_3 = 2m_3\pi + \Delta\theta, \quad (4a)$$

$$\cos\Delta\theta = \eta_1\left[1 + \frac{c_1(1/\eta_1^2 - 1)}{c_1 + 1/2}\right], \quad (4b)$$

where m_1 and m_3 are two integers. Here, Eqs. (4a) and (4b) together give the condition for the output amplitude to vanish under modulation. For Eq. (4b) to be valid (for a real phase shift $\Delta\theta$), its right hand side must be no greater than unity. Detailed calculations show that this requires $\eta_1 \geq 2c_1 = \cos\sqrt{2}\kappa L$, which clearly corresponds to the overcoupling regime for an unmodulated dual-racetrack resonator, by comparison to Eq. (3). The structure used in this work has a racetrack length $L = 3$ μm and radius $r = 3$ μm.

For a dual-racetrack resonator to produce arbitrary QAM signals, a general design goal is that its output amplitude and phase can cover the maximum area within the unit circle on the complex E_{out} plane, where all possible coherent output states reside. Furthermore, it would be desirable that such coverage is achieved efficiently through index modulation. To achieve such design goals, simply satisfying Eqs. (4a) and (4b) is not sufficient as this only ensures the coverage of the $E_{\text{out}} = 0$ point. The dependence of coverage on various parameters must be systematically analyzed.

The coherent output characteristics of a dual-racetrack resonator are largely affected by two key parameters: the coupling constant c_1 and the loss parameter η_1. The latter can be related to a more frequently used parameter quality factor $Q_n \approx \pi n_g L_{\text{tot}}/[(1 - \eta_n)\lambda]$, where n_g is the group index and L_{tot} is the round trip length of a resonator, and λ is the wavelength. We simulate the coverage of the coherent output states for Δn_1, $\Delta n_3 = -0.001$ to $+0.001$, for a number of cases with different Q_1 and c_1 parameters, as shown in Fig. 2. In plotting Fig. 2, we have defined

$$E_{\text{out}} = b_2/e^{i\phi}. \quad (5)$$

This allows us to remove an unimportant phase factor $e^{i\phi}$ whose effect is simply to shift the output phase for each device by a fixed amount. Such an overall baseline phase shift has no actual effect on the device operation. Apparently, the coverage improves for larger Q_1 and larger c_1.

To gain insight into the evolution of the coverage with device parameters, we wish to develop some analytic theory that can describe the relation between the coverage area and the key parameters Q_1 and c_1. Although the overall characteristics are complex from Fig. 2, it appears that the following features are critical. (1) The covered area is always symmetric with respect to the real axis (after removing the baseline phase shift $e^{i\phi}$). (2) The leftmost and rightmost points of the covered area are located

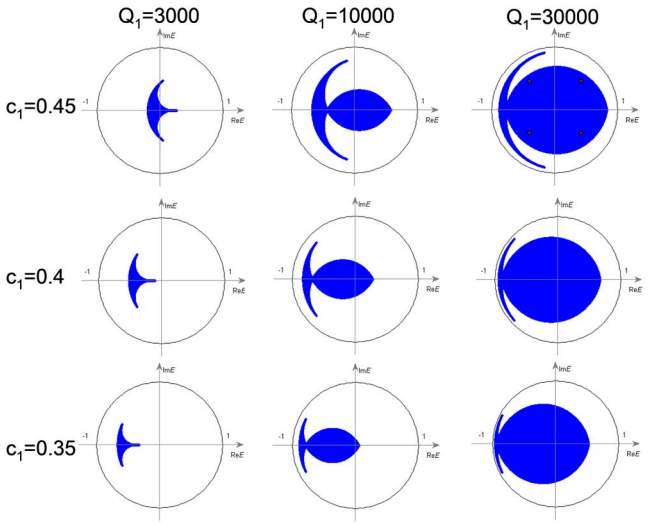

Fig. 2. Coverage of the coherent output states for Δn_1, $\Delta n_3 = -0.001 - +0.001$, under different Q_1 and c_1. A potential QPSK constellation is shown in the top right case.

on the real axis, and the covered area is largely limited by the location of the two points min Re E_{out}, max Re E_{out}. (3) As the quality factor increases, min Re E_{out} decreases and max Re E_{out} increases, hence the coverage enlarges. (4) As the coupling constant increases, both min Re E_{out} and max Re E_{out} increases. The last characteristic is interesting in that when both points increase, generally it is hard to predict the increase or decrease of the coverage area. However, it appears that in the cases shown in Fig. 2, the increase of max Re E_{out} with c_1 is faster than that of min Re E_{out}. Therefore, the coverage still improves.

Overall, it appears that the coverage is largely controlled by the two points on the real axis, min Re E_{out} and max Re E_{out}. It would be desirable to derive the formula for these two points and analyze its trend. Note that E_{out} is real if and only if $\Delta u_1 = \Delta u_3^*$, according to Eq. (1). According to the definition of Δu_n in Eq. (2), this real E_{out} requirement translates to the condition given by Eq. (4a). This can be called a push–pull condition because it requires the phase in one resonator to increase and the other to decrease. Under this push–pull condition, we find

$$\frac{1}{\Delta u_1}+\frac{1}{\Delta u_3}=2\,\mathrm{Re}\,\frac{1}{\Delta u_1}=\frac{2\cos\Delta\theta/\eta_1-2}{1/\eta_1^2+1-2\cos\Delta\theta/\eta_1}. \quad (6)$$

Note that all E_{out} on the real axis can be obtained by $E_{\text{out}}(\Delta\theta,-\Delta\theta)$. One can readily show that the minimum and maximum Re E_{out} is achieved when $\cos\Delta\theta=\pm1$,

$$\min\,\mathrm{Re}(E_{\text{out}})=\left[-1+\frac{(2c_1+1)}{(1-2c_1)/(1/\eta_1-1)+1}\right], \quad (7)$$

$$\max\,\mathrm{Re}(E_{\text{out}})=\left[-1+\frac{(2c_1+1)}{-(1-2c_1)/(1/\eta_1+1)+1}\right]. \quad (8)$$

When we compare these values with the leftmost and rightmost points on the real axis, we find that the leftmost point agrees well with Eq. (7), but the rightmost point is generally smaller than the value given by Eq. (8). This can be understood as follows. The leftmost point is achieved with $\cos\Delta\theta=1$, or $\Delta\theta=0$ when the refractive index is not modulated. The rightmost point is achieved with maximum phase shift $\Delta\theta_{\max}$. Depending on the magnitude of Δn_n, it is possible that $\Delta\theta_{\max}<\pi$. Therefore, the rightmost point in Fig. 2 is actually defined by $E_{\text{out}}(\Delta\theta_{\max},-\Delta\theta_{\max})$, where $\Delta\theta_{\max}$ is determined by the maximum Δn_n.

Therefore, the coverage of the coherent output states (on the complex E_{out} plane) is prescribed by the following analytic formula: Eq. (7) gives the leftmost point of the covered area and Eqs. (1) and (6) together give the rightmost point. We can plot $E_{\text{out}}(\Delta\theta,-\Delta\theta)$ for $\Delta\theta=0$ and $\Delta\theta=\Delta\theta_{\max}$ for various refractive index modulation levels, as shown in Fig. 3(a), and analyze their trends with the key physical parameters of quality factor and the coupling constant. For reference, the maximum Re E_{out} defined by

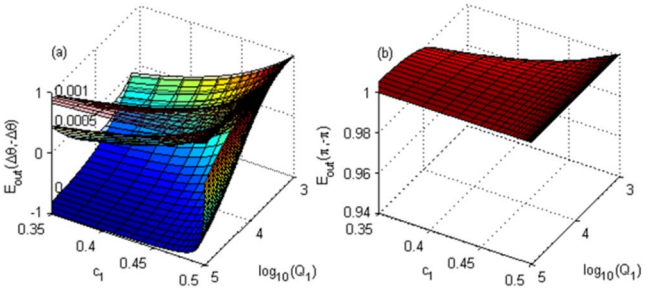

Fig. 3. Variation of the output amplitude under the condition $\Delta\theta_1=-\Delta\theta_3$ (a) for various levels of $\Delta n=0$, 0.0005, 0.001; and (b) for a phase shift $\Delta\theta_1=-\Delta\theta_3=\pi$, which gives the maximum real value of E_{out}. Note that the scale of the vertical axes in (a) and (b) are different.

$E_{\text{out}}(\pi,\pi)$ is also plotted in Fig. 3(b). However, it should be noted that this quantity is almost always close to unity, and the actual maximum $E_{\text{out}}(\Delta\theta_{\max},-\Delta\theta_{\max})$ is limited by the amount of index modulation.

Clearly, as the quality factor increases, min Re $E_{\text{out}}=E_{\text{out}}(0,0)$ decreases and $E_{\text{out}}(\Delta\theta_{\max},-\Delta\theta_{\max})$ increases, hence the covered area enlarges. This explains the trend with the quality factor given in Fig. 2. On the other hand, as the coupling constant increases, both min Re E_{out} and $E_{\text{out}}(\Delta\theta_{\max},-\Delta\theta_{\max})$ increases. For small c_1 values between 0.35 and 0.45, min Re $E_{\text{out}}=E_{\text{out}}(0,0)$ increases very slowly with c_1, which does not obviously reduce the coverage on the complex E_{out} plane. However, for $c_1>0.45$, min Re E_{out} increases very rapidly, which will significantly degrade the coverage. To better illustrate this effect, we further plot the coverage for $c_1=0.46\sim0.49$ (with $Q_1=30000$ and Δn_1, $\Delta n_3=-0.001-+0.001$) in Fig. 4. The trend with respect to c_1 at the given quality factor is plotted in Fig. 4(e) for clarity. Evidently, for too high c_1 values, $E_{\text{out}}(0,0)$ rises fast and the coverage degrades rapidly. Note that the maximum possible value of c_1 is 0.5 according to its definition. Also, increase of the quality factor is limited by the waveguide loss.

The best coverage shown in Fig. 2 can be further improved by varying the maximum index modulation.

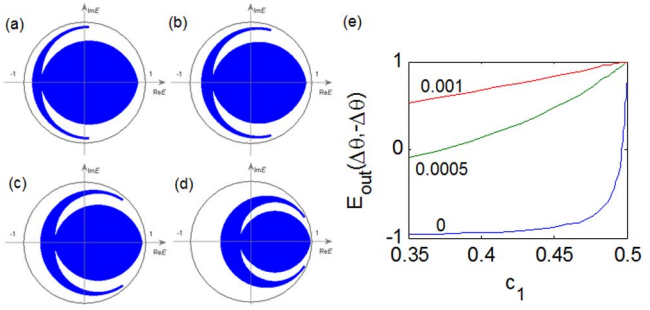

Fig. 4. Coverage of coherent output states for $Q_1=30000$ and Δn_1, $\Delta n_3=-0.001-+0.001$ (a) $c_1=0.46$, (b) $c_1=0.47$, (c) $c_1=0.48$, and (d) $c_1=0.49$. (e) $E_{\text{out}}(\Delta\theta,-\Delta\theta)$ for different c_1.

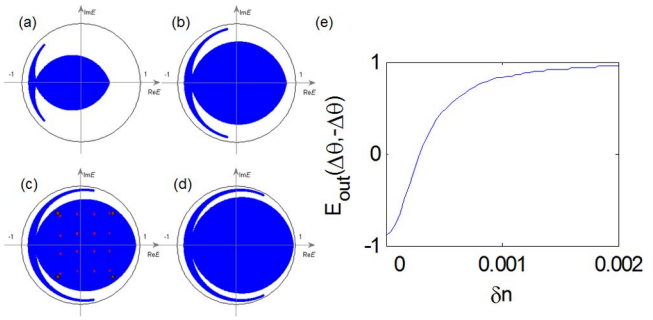

Fig. 5. Coverage of coherent output states for $Q_1 = 30000$ and $c_1 = 0.45$, for Δn_1, $\Delta n_3 = -\delta n - +\delta n$. (a) $\delta n = 0.0005$, (b) $\delta n = 0.001$, (c) $\delta n = 0.0015$, (d) $\delta n = 0.002$. (e) The variation of the $E_{\text{out}}(\Delta\theta_{\max}, -\Delta\theta_{\max})$ with δn.

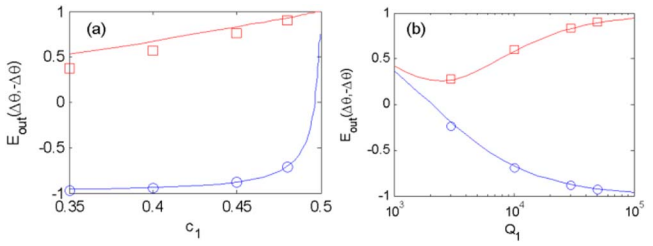

Fig. 6. Influence of the structure asymmetry in dual-racetrack resonators. The red and blue lines represent $E_{\text{out}}(0,0)$ and $E_{\text{out}}(\Delta\theta_{\max}, -\Delta\theta_{\max})$ for $\delta n = 0.001$, respectively, for an ideal structure whose parameters are the same as Fig. 5. The symbols represent the results for a structure (a) with 20% asymmetry in κ, and (b) with 20% asymmetry in the quality factor.

To this end, the coverage under various maximum index modulation levels is plotted in Figs. 5(a)–5(d). Generally, $E_{\text{out}}(\Delta\theta_{\max}, -\Delta\theta_{\max})$ increases very fast at small δn values; and the coverage somewhat saturates after $\delta n \geq 0.0015$, after which the coverage increases very slowly with δn. Figure 5(e) illustrates the overall trend with δn. Note that the coverage at $\delta n = 0.0015$ is sufficiently large, and one may use this in practical applications to avoid unnecessary further increase of the driving signal and ensure efficient operation of the device. According to the AC current formula of silicon modulators based on charge supply (or extraction)[10,11], the AC driving current for $\delta n = 0.0015$ is estimated at around 2 mA at 10 Gbaud, which is reasonable. Possible constellations for QPSK and 16-QAM are shown in Fig. 5(c).

Due to fabrication imperfections, there may exist some asymmetry between the quality factors (Q_1, Q_3) and coupling constants (κ_{12}, κ_{23}). To analyze the influence of such asymmetry, we plot the E_{out} characteristics with varying coupling constants and quality factors in Fig. 6. The symbols represent the data for 20% asymmetry between the resonators in κ or Q. Evidently, the difference between asymmetric cases and the ideal symmetric case represented by the lines is fairly small. Under such asymmetry, the above analytic results can remain quite robust, and the coverage does not deviate far from the ideal design.

In conclusion, we develop an approach to the systematic design of the dual-racetrack resonator structure for maximum coverage of the complex output E-field plane in order to generate quadrature amplitude signals. The trend of coverage with varying quality factor and varying coupling constant is systematically analyzed. As the quality factor increases, the coverage is improved. As the coupling constant increases, the coverage initially increases then degrades. The influence of the level of refractive index modulation is found to saturate after reaching a certain level. The design results are reasonably robust against a small asymmetry of the device parameters.

This work was supported in part by the Jiangsu Province Natural Science Foundation of China (No. BK20141168) and the Jiangsu Overseas Research & Training Program for University Prominent Young & Middle-aged Teachers and Presidents.

References

1. P. J. Winzer and R.-J. Essiambre, J. Lightwave Technol. **24**, 4711 (2006).
2. Q. F. Xu, B. Schmidt, S. Pradhan, and M. Lipson, Nature **435**, 325 (2005).
3. C. Li, L. J. Zhou, and A. W. Poon, Opt. Express **15**, 5069 (2007).
4. D. M. Gill, S. S. Patel, M. Rasras, K. Y. Tu, A. E. White, Y. K. Chen, A. Pomerene, D. Carothers, R. L. Kamocsai, C. M. Hill, and J. Beattie, IEEE J. Sel. Top. Quantum Electron. **16**, 45 (2010).
5. Z. Zhou, Z. Tu, B. Yin, W. Tan, L. Yu, H. Yi, and X. Wang, Chin. Opt. Lett. **11**, 012501 (2013).
6. X. Xiao, H. Xu, X. Li, Y. Hu, K. Xiong, Z. Li, T. Chu, Y. Yu, and J. Yu, Opt. Express **20**, 2507 (2012).
7. L. Zhang, J.-Y. Yang, Y. Li, M. Song, R. G. Beausoleil, and A. E. Willner, Opt. Lett. **33**, 1428 (2008).
8. P. Dong, C. Xie, L. Chen, N. K. Fontaine, and Y.-K. Chen, Opt. Lett. **37**, 1178 (2012).
9. R. A. Integlia, L. Yin, D. Ding, D. Z. Pan, D. M. Gill, and W. Jiang, Opt. Express **19**, 14892 (2011).
10. L. Gu, W. Jiang, X. Chen, L. Wang, and R. T. Chen, Appl. Phys. Lett. **90**, 071105 (2007).
11. W. Jiang, L. Gu, X. Chen, and R. T. Chen, Solid-State Electron. **51**, 1278 (2007).